The Astrophysical Journal, 975:171 (13pp), 2024 November 10 https://doi.org/10.3847/1538-4357/ad7841

KIC 8840638: A Newly Discovered Eclipsing Binary with δ Scuti–Type Oscillations

Tao-Zhi Yang[1], Zhao-Yu Zuo[1], Jun-Hui Liu[2,3], Deng-Kai Jiang[4,5,6,7], Zhi-Xiang Zhang[2], Qin-jie Tang[1], and Antonio García Hernández[8]

[1] Ministry of Education Key Laboratory for Nonequilibrium Synthesis and Modulation of Condensed Matter, School of Physics, Xi'an Jiaotong University, 710049 Xi'an, People's Republic of China; zuozyu@xjtu.edu.cn
[2] Department of Astronomy, Xiamen University, 361005 Xiamen, Fujian, People's Republic of China; liujunhui@stu.xmu.edu.cn
[3] Research School of Astronomy & Astrophysics, Australian National University, Cotter Road, Weston, ACT 2611, Australia
[4] Yunnan Observatories, Chinese Academy of Sciences, 396 Yangfangwang, Guandu District, Kunming 650216, People's Republic of China
[5] Center for Astronomical Mega-Science, Chinese Academy of Sciences, 20A Datun Road, Chaoyang District, Beijing 100012, People's Republic of China
[6] Key Laboratory for the Structure and Evolution of Celestial Objects, Chinese Academy of Sciences, Kunming 650011, People's Republic of China
[7] International Centre of Supernovae, Yunnan Key Laboratory, Kunming 650216, People's Republic of China
[8] Departamento de Física Teórica y del Cosmos, Universidad de Granada, Campus de Fuentenueva s/n, E-18071, Granada, Spain
Received 2023 October 12; revised 2024 September 5; accepted 2024 September 6; published 2024 October 31

Abstract

In this paper, we analyze the light variation of KIC 8840638 using high-precision time-series data from the Kepler mission. The analysis reveals that this target is a new detached eclipsing binary system with a δ Scuti component, rather than a single δ Scuti star as previously known. The frequency analysis of short-cadence data reveals 95 significant frequencies, most of which lie in a frequency range of $23-32\,\mathrm{day}^{-1}$. Among them, seven independent frequencies are detected in the typical frequency range of δ Scuti stars, and they are identified as pressure modes. In addition, a possible large separation value of $\Delta\nu = 36.5 \pm 0.1\ \mu$Hz is also detected with the Fourier transform (FT) and autocorrelation function (AC) analysis. The orbital frequency f_{orb} ($= 0.320008\,\mathrm{day}^{-1}$) and its harmonics are also detected directly in the frequency spectrum. The binary modelings derived from PHOEBE indicate that this binary system is in detached configurations with a mass ratio of $q = 0.33^{+0.06}_{-0.04}$, an inclination angle of $40.19^{+3.96}_{-2.84}$°. The derived parameters and binary evolutionary model suggest that the primary star is an object on the verge of leaving the main sequence with a temperature of ∼7600 K, while the secondary appears to be a cool component entering the giant branch with a temperature ∼3100 K lower than the primary. Moreover, this system may have undergone a mass ratio reversal, where the more massive star is the gainer component and the less massive one is the donor star.

Unified Astronomy Thesaurus concepts: Delta Scuti variable stars (370); Stellar oscillations (1617); Short period variable stars (1453); Eclipsing binary stars (444)

1. Introduction

Eclipsing binaries (EBs) are primary targets for us to obtain precise fundamental stellar parameters (D. M. Popper 1980; G. Torres et al. 2010). With high-precision time-series photometric and spectroscopic observations, the mass and radius of each component in EBs can be determined precisely within 1% (J. Southworth et al. 2005; J. V. Clausen et al. 2008). Additionally, with high-precision and long-term photometric time series, the mideclipse times can also be determined. These timing measurements can be used to find more components and/or investigate a variety of different physical phenomena causing the orbital period changes of EBs (R. W. Hilditch 2001; J. M. Kreiner et al. 2001).

EBs consisting of a pulsating member have attracted great scientific interest during the past two decades, as not only could the stellar parameters of each star be obtained in binaries, but also the internal structure of pulsating stars could be studied simultaneously with asteroseismology by exploring high-precision photometric observations. Among the pulsating EBs, about 208 systems have been classified as δ Sct–type EBs, which were also called "oscillating eclipsing Algol (oEA) stars" (D. E. Mkrtichian et al. 2004; A. Liakos & P. Niarchos 2017; A. Liakos 2018). δ Sct stars are short-period pulsators with periods in the range of 0.02–0.25 day (M. Breger 2000). They are located at the intersection of the main sequence and classical Cepheid instability strip, and the spectral type is from A2 to F5 (E. Rodríguez & M. Breger 2001). They usually pulsate in low-order radial/nonradial pressure (p) modes due to a κ mechanism acting in the partial ionization of He II. These pulsations can be used to probe the envelope of a star with asteroseismology (G. Houdek et al. 1999). The δ Sct components in binaries share some similar features with single δ Sct stars, but the pulsations in oEA might be influenced by the companion due to mass transfer and gravitational forces from the companion (E. Soydugan et al. 2006). In addition, a threshold in the orbital period of about 13 days was found by A. Liakos & P. Niarchos (2015, 2016). Below this threshold, the pulsations would be influenced by the binarity. X. B. Zhang et al. (2013) investigated the relation between orbital and pulsation periods from a theoretical perspective and found that the pulsations in EBs depend on multiple factors, i.e., the system's orbital period, the mass ratio of the binary system, and the filling factor of the primary pulsating member. Moreover, the tidal excited modes have also been found in eccentric-orbit binaries, and the resulting excited modes appear as the frequencies at multiples of the orbital frequency (W. F. Welsh et al. 2011; K. M. Hambleton et al. 2013).

Table 1
Basic Parameters of KIC 8840638

Parameters	KIC 8840638	References
P	49.6 minutes	(a)
$T_{\rm KIC}$	6310 ± 250 K	(b)
$T_{\rm GTC}$	7860 ± 120 K	(a)
$\log g$	3.86 ± 0.25 dex	(c)

Note. (a) G. Ramsay et al. (2014); (b) KIC (T. M. Brown et al. 2011); (c) https://gea.esac.esa.int/archive/. Note that the KIC temperatures are systematically smaller than other temperature determinations (D. Huber et al. 2014), while $T_{\rm GTC}$ is determined from spectroscopy (INT + GTC spectra obtained at Obs. Roque de los Muchachos, La Palma; G. Ramsay et al. 2014).

Recently, some pulsating EBs located in special evolutionary stages have also been reported. For example, KIC 10736223 was reported to be a pulsating Algol system that has just undergone a rapid mass-transfer process (X. Chen et al. 2020), and so was OO Dra, another similar system to KIC 10736223 with a rapid mass transfer (X. Chen et al. 2021).

Thanks to the ultra-high-precision photometric observations, the Kepler mission (W. J. Borucki et al. 2010; D. G. Koch et al. 2010) has found more than 2878 EB systems (B. Kirk et al. 2016) and at least 2000 δ Sct stars in the main field of view so far (L. A. Balona & W. A. Dziembowski 2011; L. A. Balona 2014; D. M. Bowman et al. 2016; T. Yang et al. 2018; T.-Z. Yang & A. Esamdin 2019; T.-Z. Yang et al. 2021, 2022; X.-Y. Sun et al. 2023). Although many researchers have been hunting for and characterizing the pulsating EBs with Kepler data, there are only about 30 new pulsating EBs with detailed investigation using Kepler data (J. W. Lee et al. 2016; Z. Guo et al. 2017; F. Kahraman Alicavus et al. 2017; J. W. Lee et al. 2017; A. Liakos & P. Niarchos 2017; A. Liakos 2018; J. W. Lee et al. 2019; X. Chen et al. 2020). The interactions between pulsations and orbital motions are still not fully understood. Very recently, X. Chen et al. (2022) systematically searched δ Sct–type pulsations in 6431 EBs (orbital periods < 13 days) based on 2 minute cadence TESS data and reported 143 new pulsating EBs. These new samples provide a great opportunity for investigating stellar parameters in detail and further addressing the issues mentioned above.

KIC 8840638 ($\alpha_{2000} = 19^{\rm h}55^{\rm m}35\overset{\rm s}{.}03$, $\delta_{2000} = +45°04'45\overset{''}{.}4$, 2MASS J19553503+4504454) was classified as a δ Scuti star by G. Ramsay et al. (2014) according to its highest peak of the frequency spectra. Its pulsating period is about 49.6 minutes, and this target was considered as a mid-to-late A-type star in that survey (G. Ramsay et al. 2014). Table 1 lists some basic parameters of KIC 8840638 collected from the survey and Kepler Input Catalog (KIC; T. M. Brown et al. 2011). However, compared with a typical single δ Scuti star whose light curve includes only pulsations, KIC 8840638 shows obviously different features; that is to say, its light curve shows a superposition of pulsations and an additional cyclic variation (as shown in the top panel of Figure 1) that could be due to the presence of eclipses of an EB system. In this paper, we further investigate its light variation and astrophysical features using the high-precision Kepler photometric time-series data. To avoid the Nyquist aliases detected in the frequency spectrum, only short-cadence (SC; integration time of 58.85 s) data were used in this work.

2. Observations and Data Reduction

KIC 8840638 was observed by the Kepler space telescope in SC from BJD 2456139.15 to 2456414.59, which spans 275.44 days. There are four quarters (Q14.2, Q15.2, Q16.2, and Q17.1) of the SC data, containing 165,143 points in total. The SC photometric flux data of KIC 8840638 are available in the Kepler Asteroseismic Science Operations Center (KASOC) database[9] (H. Kjeldsen et al. 2010) with two types: the first is labeled as "raw" data, which were produced by the NASA Kepler Science pipeline, and the second is the flux data corrected by KASOC Working Group 4 (δ Scuti targets). We use the corrected data and perform corrections eliminating outliers, as well as the possible linear trends in some quarters. The flux data are converted to the magnitude scale, the mean value of each quarter is subtracted, and the rectified time series is obtained. Figure 1 shows the rectified light curve of KIC 8840638 in SC data. It is clear that its light curve shows a superposition of pulsations (bottom panel of Figure 1) and an additional cyclic variation (top panel of Figure 1) that could be due to the presence of eclipses of an EB system.

3. Pulsational Characteristics

To investigate the pulsating behavior of KIC 8840638, we used the software PERIOD04 (P. Lenz & M. Breger 2005) to perform Fourier analysis for the rectified data. To detect more significant frequencies in the SC data, we chose a frequency range of $0\ {\rm day}^{-1} < \nu < 80\ {\rm day}^{-1}$, a little wider than the typical pulsation frequency range of δ Sct stars.

During the extraction of significant frequency, the highest peak in the frequency spectrum was considered as a significant frequency; then a multifrequency least-squares fit using the formula $m = m_0 + \Sigma {\rm A}_i \sin(2\pi({\rm f}_i{\rm t} + \phi_i))$ (where m_0 is the zero-point, A_i is the amplitude, f_i is the frequency, and ϕ_i is the corresponding phase) was conducted to the light curve with all the significant frequencies detected, resulting in the solutions of all the significant frequencies. A constructed light curve using the above solutions was subtracted from the data, and the residual was obtained to search for the next significant frequency. Then, the above steps were repeated until there was no significant peak in the frequency spectrum. The criterion (S/N > 4.0) suggested by M. Breger et al. (1993) was adopted to judge the significant peaks. The uncertainties of the frequencies were calculated following T. Kallinger et al. (2008).

A total of 95 significant frequencies were extracted, and they are listed in Table 2. Figure 2 shows the amplitude spectra of KIC 8840638. Note that most of the detected frequencies lie in a frequency region between 23.0 and 32.0 day^{-1}. Among these frequencies, seven strong frequencies, i.e., f_2, f_4–f_8, and f_{19}, are considered to be independent frequencies, as they are neither combinations nor harmonics of other frequencies. These seven frequencies are marked with "independent" in the last column of Table 2. Only several frequencies can be easily identified as combinations with a simple form $(f \pm \sigma) = m(f_1 \pm \sigma_1) \pm n(f_2 \pm \sigma_2)$ using the Rayleigh criterion ($1/\Delta T = 0.003$ c day^{-1}), where m and n are small integers, f_1 and f_2 are the stronger frequencies, and we denoted their identifications. Among these frequencies, there are nine combinations (i.e., f_9, f_{13}, f_{31}, f_{38}, f_{52}, f_{53}, f_{59}, f_{64}, and f_{73}) with $f_{\rm orb}$ coupled to f_5 and f_7, as shown in panel (b) of Figure 2. For most frequencies without identification,

[9] KASOC database: http://kasoc.phys.au.dk.

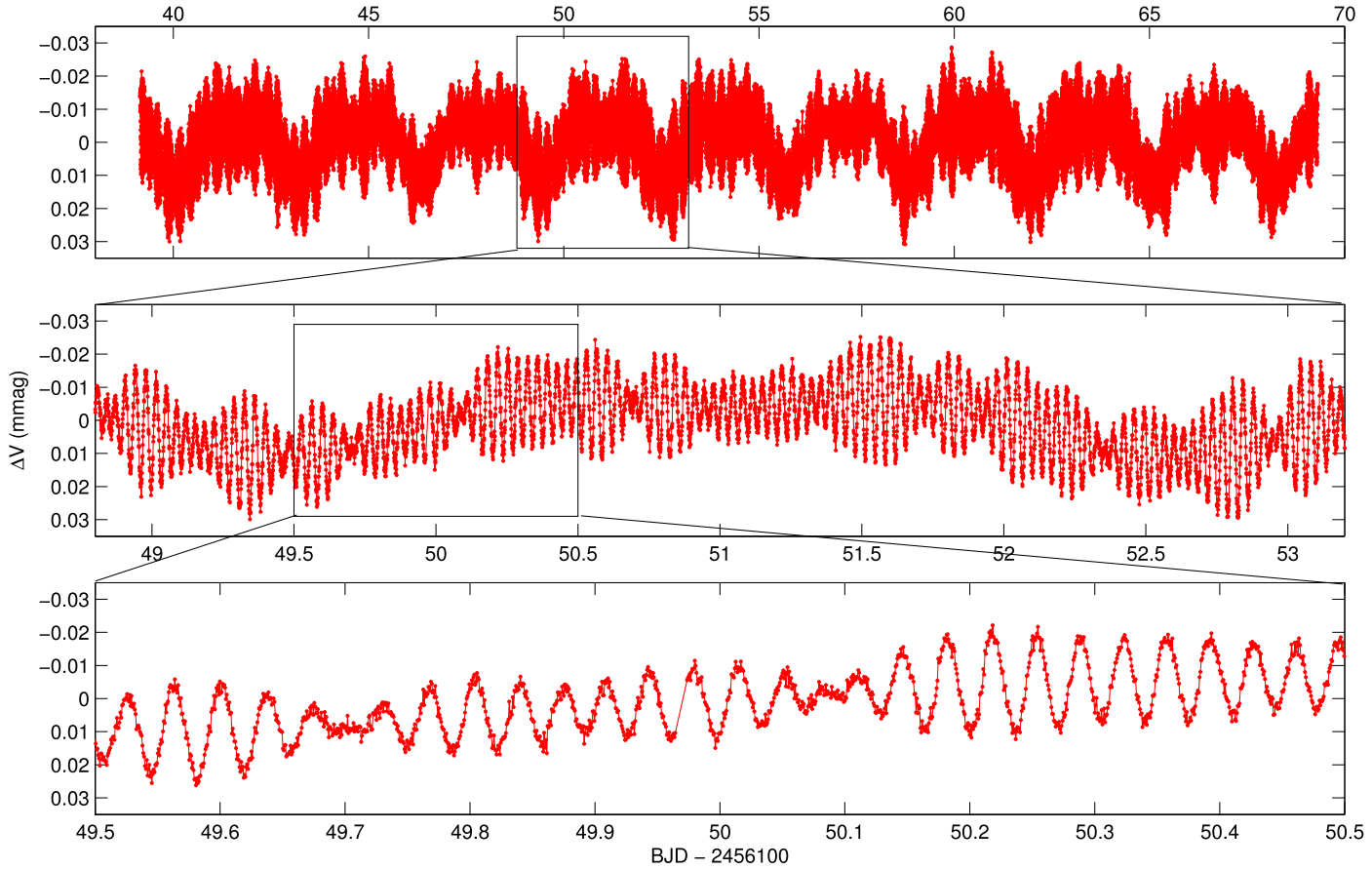

Figure 1. The light curve of KIC 8840638 in SC. Top panel: the whole light curve of Q14.2. Middle panel: the zoom-in light curve of Q14.2 with 4.4 days. Bottom panel: the zoom-in light curve of Q14.2 with 1.0 day.

their forms of combination are very complicated and hence may be just a coincidence.

In the low-frequency region of 0 $\text{day}^{-1} < \nu < 1\ \text{day}^{-1}$, three frequencies, f_1(=0.320008 day^{-1}), f_3(=0.639945 day^{-1}), and f_{62}(=0.959744 day^{-1}), are interesting peaks. We examined these frequencies and found that f_3 and f_{62} are harmonics of f_1. The lowest frequency, f_1, was likely due to the orbital motion of the binary. In the frequency region of 35 $\text{day}^{-1} < \nu < 80\ \text{day}^{-1}$, several peaks were detected, and they mainly concentrate in a narrow region of 52 $\text{day}^{-1} < \nu < 58\ \text{day}^{-1}$. These frequencies are combinations and harmonics of the independent terms and the orbital frequency.

4. Binary Modeling

From the top and middle panels of Figure 1, the light variation of KIC 8840638 exhibits the typical shapes of the light curve of EBs, suggesting that this target should belong to a binary system containing a pulsating component. To clearly show light variations due to the orbital motion from the binary, the light curve is folded with the detected low frequency of f_1. Figure 3 shows the phase diagram of SC data, which includes 100 time bins. From this figure, the orbital phase diagram of KIC 8840638 is clearly shown, so the lowest frequency f_1 was marked as the orbital frequency (denoted as "$f_{\rm orb}$") in Table 2.

To obtain the physical and geometrical parameters of this binary system, we use the PHysics Of Eclipsing BinariEs (PHOEBE) 2.3 package (A. Prša & T. Zwitter 2005; A. Prša et al. 2016) to analyze the rectified SC data. PHOEBE has advanced algorithms for calculating the light curves and radial velocity curves of EB systems, as well as tools for fitting comprehensive physical models to observational data, including gravitational interaction, tidal distortion, and mass transfer. Its built-in Markov Chain Monte Carlo (MCMC) module allows users to perform MCMC-based parameter estimation for EB systems. The module uses the emcee (an MCMC algorithm; D. Foreman-Mackey et al. 2013) package to sample the posterior probability distribution of the parameters, which allows for uncertainty estimation and robust parameter determination. Considering that multiperiodic pulsations could affect the solution of the observed light curve and that running the PHOEBE model calculation is very time-consuming, the removal of pulsating signals will be more conducive to the solution of binary parameters by PHOEBE. Thus, all the pulsating signals in the light curve were first smoothed out using half of the strongest pulsation frequency (f_2), leaving only the light variations due to the orbital motion from the binary.

To get the temperature prior for the subsequent PHOEBE fitting, we use the broadband spectral energy distribution (SED) fitting to constrain the temperature of this target. In the SED fitting, we utilize the BT-Settl (F. Allard et al. 2012) synthetic spectral library to predict the bandpass-averaged magnitudes, while the spectral models are interpolated by the package `stellarSpecModel`.[10] The MCMC Ensemble sampler `emcee` (D. Foreman-Mackey et al. 2013) is employed

[10] https://github.com/zzxihep/stellarSpecModel

Table 2
All Frequencies Detected in SC Data

f_i	Frequency (day^{-1})	Amplitude (mmag)	S/N	Identification
1	0.320008 ± 0.000001	7.989	42.2	f_{orb}
2	29.024570 ± 0.000001	7.697	85.0	Independent
3	0.639945 ± 0.000003	4.252	77.3	$2f_{orb}$
4	25.843653 ± 0.000003	3.780	36.3	Independent
5	24.985826 ± 0.000005	2.441	30.3	Independent
6	28.925876 ± 0.000005	2.205	35.0	Independent
7	24.110686 ± 0.000006	2.032	45.6	Independent
8	27.365182 ± 0.000008	1.408	13.5	Independent
9	25.625751 ± 0.000008	1.401	39.0	f_5+2f_{orb}
10	28.286089 ± 0.000009	1.218	18.8	f_6-2f_{orb}
11	28.225151 ± 0.000011	1.074	17.8	$f_4+f_8-f_5$
12	27.229833 ± 0.000012	0.944	12.7	$2f_6-f_2-5f_{orb}$
13	23.470778 ± 0.000014	0.837	28.9	f_7-2f_{orb}
14	26.725303 ± 0.000018	0.652	9.5	f_8-2f_{orb}
15	27.636970 ± 0.000018	0.650	11.5	⋯
16	27.215143 ± 0.000018	0.651	12.8	$f_6+2f_5-2f_4$
17	28.865007 ± 0.000021	0.541	16.2	⋯
18	26.934483 ± 0.000022	0.521	10.6	⋯
19	24.099312 ± 0.000022	0.520	20.5	Independent
20	27.254431 ± 0.000025	0.467	9.8	⋯
21	26.637981 ± 0.000029	0.390	8.5	⋯
22	26.415518 ± 0.000031	0.369	9.0	⋯
23	26.997106 ± 0.000037	0.307	8.3	⋯
24	24.520008 ± 0.000040	0.290	14.7	⋯
25	23.459362 ± 0.000044	0.262	18.1	$f_4+f_5-f_8$
26	27.205488 ± 0.000049	0.236	6.6	⋯
27	25.676200 ± 0.000055	0.211	8.0	⋯
28	30.494036 ± 0.000057	0.203	12.8	⋯
29	26.553998 ± 0.000058	0.198	6.0	$f_6+f_7-f_4-2f_{orb}$
30	28.395747 ± 0.000064	0.181	6.1	⋯
31	26.351489 ± 0.000068	0.170	5.7	f_7+7f_{orb}
32	27.277842 ± 0.000069	0.167	5.0	⋯
33	23.845839 ± 0.000071	0.163	11.4	⋯
34	25.890555 ± 0.000070	0.164	7.0	⋯
35	27.574478 ± 0.000072	0.160	5.0	⋯
36	25.036422 ± 0.000077	0.150	8.5	⋯
37	27.055648 ± 0.000078	0.148	6.0	⋯
38	26.669568 ± 0.000078	0.147	5.5	f_7+8f_{orb}
39	27.955661 ± 0.000081	0.142	5.0	⋯
40	27.907678 ± 0.000077	0.149	5.7	$f_4+f_8-f_5-f_{orb}$
41	27.208304 ± 0.000082	0.141	5.6	⋯
42	26.476246 ± 0.000082	0.140	6.3	⋯
43	58.049048 ± 0.000082	0.140	17.3	$2f_2$
44	56.152527 ± 0.000088	0.130	10.5	$f_5+f_6+7f_{orb}$
45	28.715414 ± 0.000095	0.121	5.4	⋯
46	24.165708 ± 0.000094	0.122	8.9	⋯
47	27.316678 ± 0.000095	0.121	5.7	⋯
48	25.250567 ± 0.000096	0.120	7.5	⋯
49	54.868095 ± 0.000101	0.114	9.6	f_2+f_4
50	23.387329 ± 0.000101	0.114	11.1	⋯
51	23.525758 ± 0.000106	0.108	11.3	⋯
52	27.309647 ± 0.000107	0.107	5.2	f_7+10f_{orb}
53	27.550568 ± 0.000114	0.101	5.0	f_5+8f_{orb}
54	28.670572 ± 0.000114	0.101	5.0	⋯
55	28.998015 ± 0.000117	0.098	5.9	⋯
56	27.109034 ± 0.000121	0.095	5.6	⋯
57	26.148543 ± 0.000125	0.092	5.2	$f6+f5-f4-6f_{orb}$
58	28.030988 ± 0.000128	0.090	4.4	⋯
59	26.910598 ± 0.000129	0.089	5.3	f_5+6f_{orb}
60	26.089366 ± 0.000135	0.085	5.8	f_8-4f_{orb}
61	26.530479 ± 0.000135	0.085	5.2	⋯
62	0.959744 ± 0.000140	0.082	4.1	$3f_{orb}$
63	23.927733 ± 0.000140	0.082	7.7	⋯
64	25.711425 ± 0.000140	0.082	5.7	f_7+5f_{orb}
65	28.293114 ± 0.000140	0.082	4.6	f_6-2f_{orb}
66	29.033747 ± 0.000146	0.079	4.2	⋯
67	56.106080 ± 0.000149	0.077	6.6	⋯
68	24.610641 ± 0.000158	0.073	5.9	⋯
69	54.571444 ± 0.000164	0.070	6.2	⋯
70	29.132862 ± 0.000164	0.070	4.2	⋯
71	26.788611 ± 0.000169	0.068	4.4	⋯
72	24.805965 ± 0.000169	0.068	5.5	⋯
73	25.305529 ± 0.000177	0.065	5.5	f_5+f_{orb}
74	22.674102 ± 0.000198	0.058	7.8	⋯
75	52.622924 ± 0.000202	0.057	5.4	⋯
76	55.923463 ± 0.000205	0.056	4.9	⋯
77	29.453077 ± 0.000205	0.056	4.1	⋯
78	25.342924 ± 0.000209	0.055	4.8	⋯
79	53.911772 ± 0.000209	0.055	4.9	f_5+f_6
80	54.634252 ± 0.000221	0.052	4.7	⋯
81	52.385486 ± 0.000225	0.051	5.0	$f_6+f_4+f_5-f_8$
82	4.815395 ± 0.000225	0.051	6.7	f_6-f_7
83	54.009898 ± 0.000230	0.050	4.7	f_2+f_5
84	55.650909 ± 0.000235	0.049	4.5	$f_6+f_8-2f_{orb}$
85	3.181020 ± 0.000235	0.049	5.0	f_2-f_4
86	19.483597 ± 0.000235	0.049	6.9	⋯
87	24.027238 ± 0.000235	0.049	5.4	⋯
88	52.660710 ± 0.000250	0.046	4.3	⋯
89	57.950430 ± 0.000256	0.045	5.0	f_2+f_6
90	25.186838 ± 0.000256	0.045	4.2	⋯
91	55.556078 ± 0.000267	0.043	4.1	⋯
92	56.702608 ± 0.000274	0.042	4.3	⋯
93	56.028777 ± 0.000274	0.042	4.0	⋯
94	52.560506 ± 0.000274	0.042	4.4	⋯
95	11.278539 ± 0.000280	0.041	5.6	$3f_{12}-3f_{13}$

to sample different parameters, mainly including temperature, radius, and extinction. We assume the E. L. Fitzpatrick (1999) extinction law with a canonical interstellar reddening law $R_V = 3.1$ (J. A. Cardelli et al. 1989). For this target, we adopt the three-dimensional reddening map from G. M. Green et al. (2019) to acquire the color excess values $E(B-V) = 0.35$ ($A_V = 3.1 \times 0.35 = 1.085$ mag). The log g for both components are assumed as 4.0 because the SEDs are weakly sensitive to surface gravity (K. El-Badry & H.-W. Rix 2022). The parallax 0.315 ± 0.013 mas from Gaia DR3 (Gaia Collaboration et al. 2023) is treated as the prior of distance. As listed in Table 3, sorted from shortest to longest central wavelengths, we collect the multiband photometric observations from UCAC4 (B and V bands; N. Zacharias et al. 2012, 2013), the Sloan Digital Sky Survey (SDSS; g_{SDSS}, r_{SDSS}, and i_{SDSS} bands; K. N. Abazajian et al. 2009; A. A. Henden et al. 2015), Pan-STARRS (g_{PS}, i_{PS}, z_{PS}, and y_{PS} bands; K. C. Chambers et al. 2016), Gaia DR3 (G_{BP}, G, and G_{RP} bands; Gaia Collaboration 2022, in preparation; Gaia Collaboration et al. 2023), TESS (K. G. Stassun et al. 2019), the Two Micron All Sky Survey (2MASS; J, H, and Ks bands; M. F. Skrutskie et al. 2006), and ALLWISE (W1 and W2 bands; R. M. Cutri et al. 2021). The entire system temperature represented by T_{GTC} (Table 1) is used as a prior for the SED fitting, with the prior modeled as a normal distribution with $\mu = 7860$ K and $\sigma = 120$ K.

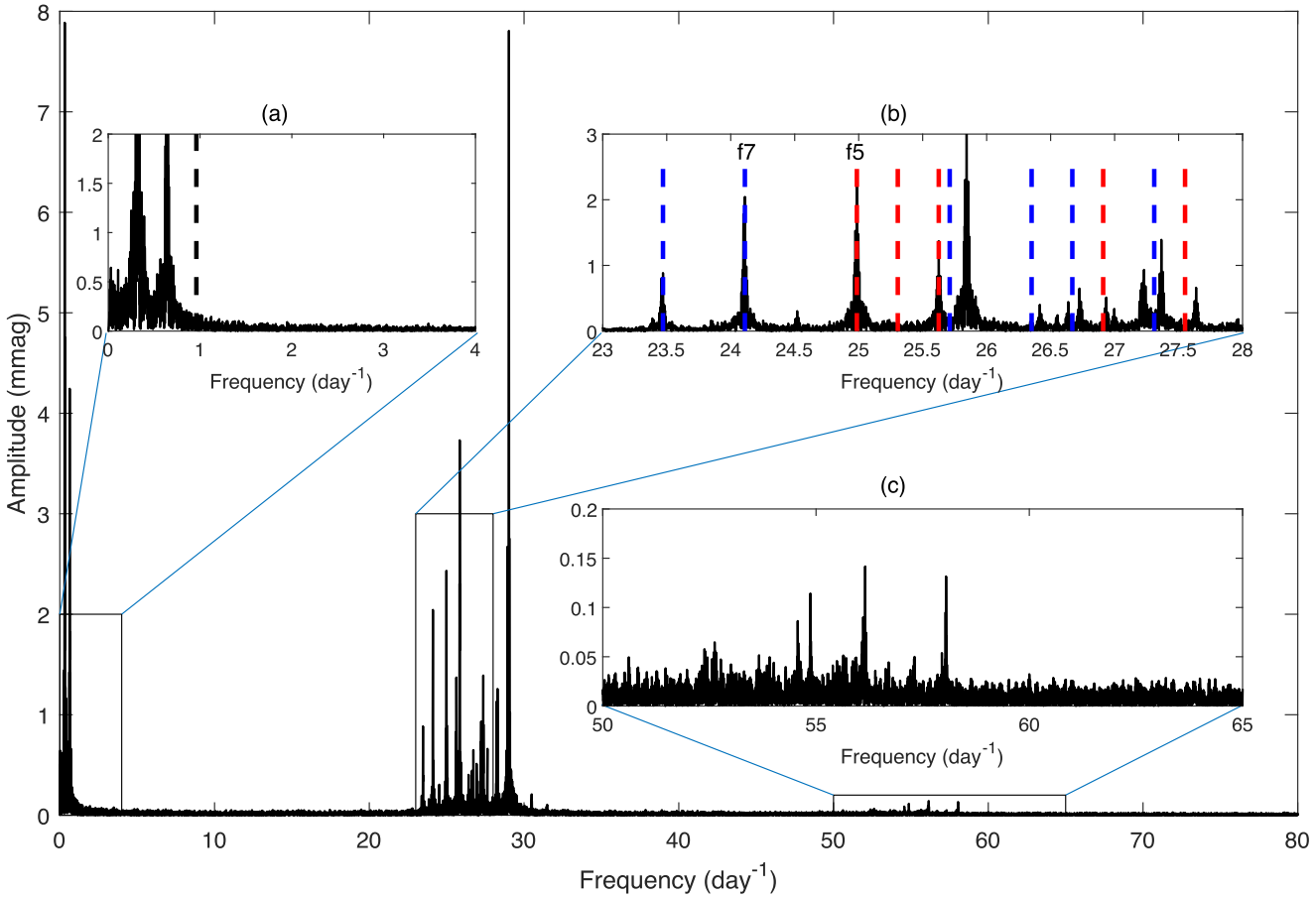

Figure 2. Amplitude spectra for the rectified SC data of KIC 8840638 up to 80 day^{-1}. (a) A zoom-in amplitude spectrum in the low-frequency region of 0 $\mathrm{day}^{-1} < \nu < 4\ \mathrm{day}^{-1}$. (b) A zoom-in amplitude spectrum in the high-frequency region of 23 $\mathrm{day}^{-1} < \nu < 28\ \mathrm{day}^{-1}$; red (blue) dashed lines indicate f_5 (f_7) and combinations with f_{orb}. (c) A zoom-in amplitude spectrum in the high-frequency region of 50 $\mathrm{day}^{-1} < \nu < 65\ \mathrm{day}^{-1}$.

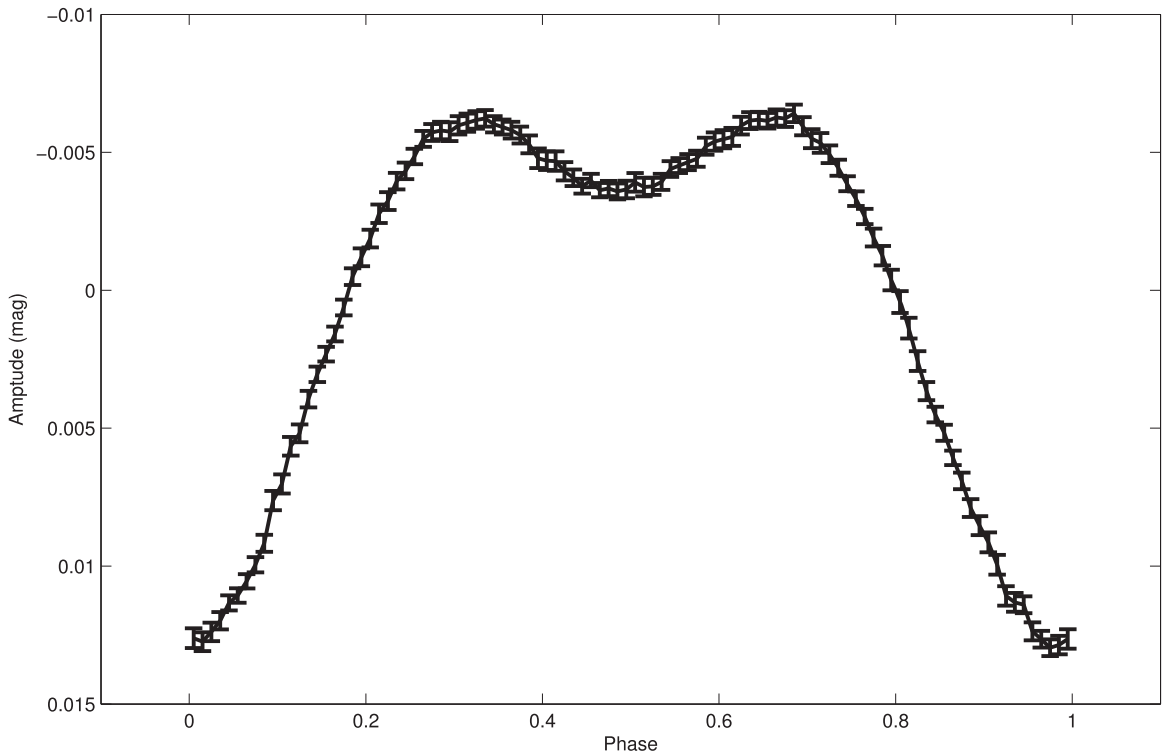

Figure 3. The folded orbital phase diagram of KIC 8840638 with the detected frequency f_1. One hundred time bins are shown in an orbital phase.

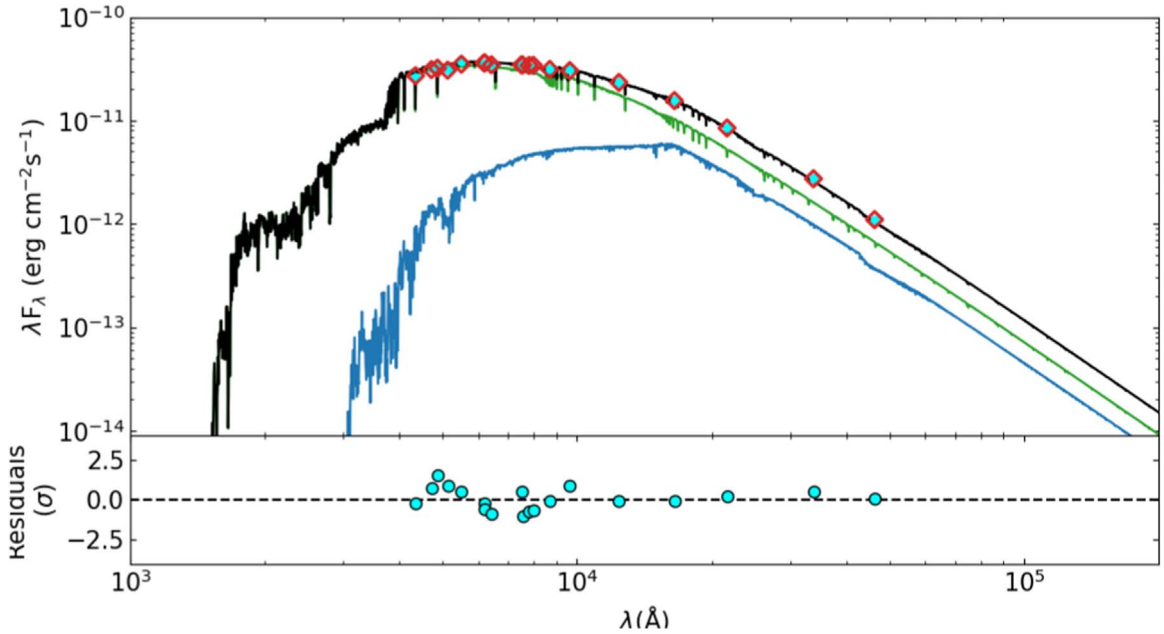

Figure 4. The SED fitting result. Upper panel: cyan points are the observed fluxes, and red diamonds are the synthetic fluxes. The black spectrum is the best-fit SED model, while the green and blue curves are the model spectra of primary and secondary stars, respectively. Lower panel: the residuals of SED fitting. The photometric observations in different bands are sorted in the order of Table 3.

Table 3
The Observational Magnitudes of KIC 8840638 in Different Bands

Bands	M_{obs} (mag)	σ_M (mag)	References
B	15.034	0.036	(1)
g_{SDSS}	14.636	0.021	(2)
g_{PS}	14.569	0.003	(3)
G_{BP}	14.536	0.004	(4)
V	14.315	0.024	(1)
r_{SDSS}	14.235	0.029	(2)
r_{PS}	14.254	0.005	(3)
G	14.216	0.003	(4)
i_{SDSS}	14.010	0.058	(2)
i_{PS}	14.103	0.004	(3)
G_{RP}	13.717	0.004	(4)
TESS	13.803	0.011	(5)
z_{PS}	14.015	0.006	(3)
y_{PS}	13.898	0.002	(3)
J	13.053	0.027	(6)
H	12.708	0.033	(6)
Ks	12.582	0.023	(6)
W1	12.494	0.023	(7)
W2	12.529	0.023	(7)

References. (1) N. Zacharias et al. (2012), UCAC4; (2) A. A. Henden et al. (2015), SDSS; (3) K. C. Chambers et al. (2016), Pan-STARRS; (4) Gaia Collaboration (2022, in preparation), Gaia DR3; (5) K. G. Stassun et al. (2019), TESS; (6) M. F. Skrutskie et al. (2006), 2MASS; (7) R. M. Cutri et al. (2021), ALLWISE.

Table 4
The Prior and PHOEBE Fitting Results for the Orbital and Stellar Parameters for KIC 8840638

Parameters	Prior	Fitting Result
A_1	1.0	/
A_2	0.5	/
g_1	$\mathcal{U}(0.1, 1.0)$	$0.38^{+0.38}_{-0.22}$
g_2	$\mathcal{U}(0.1, 1.0)$	$0.34^{+0.10}_{-0.11}$
i (deg)	$\mathcal{U}(0, 90)$	$40.19^{+3.96}_{-2.84}$
q	$\mathcal{U}(0.1, 10)$	$0.33^{+0.06}_{-0.04}$
a ($R_\odot$)	$\mathcal{U}(0.5, 100)$	$12.10^{+0.30}_{-0.40}$
R_1 ($R_\odot$)	$\mathcal{U}(1.1, 3.0)$	$2.92^{+0.14}_{-0.14}$
R_2 ($R_\odot$)	$\mathcal{U}(0.3, 10.0)$	$3.13^{+0.18}_{-0.18}$
T_1 (K)	$\mathcal{N}(7700, 200)$	$7638.18^{+198.68}_{-124.68}$
T_2 (K)	$\mathcal{N}(4400, 200)$	$4452.15^{+142.71}_{-138.16}$
M_1 ($M_\odot$)	/	$1.82^{+0.12}_{-0.18}$
M_2 ($M_\odot$)	/	$0.60^{+0.10}_{-0.08}$
log g_1 (dex)	/	$3.76^{+0.04}_{-0.05}$
log g_2 (dex)	/	$3.23^{+0.05}_{-0.04}$
L_1 ($L_\odot$)	/	$26.31^{+4.02}_{-3.12}$
L_2 ($L_\odot$)	/	$3.43^{+0.57}_{-0.48}$
fi_1 (%)	/	58^{+3}_{-3}
fi_2 (%)	/	89^{+3}_{-4}

Note. $\mathcal{U}(a, b)$ means the uniform distribution from a to b. $\mathcal{N}(c, d)$ means the Gaussian distribution with the expectation $\mu = c$ and standard deviation $\sigma = d$. / means the values are fixed during fitting and no prior values, respectively.

The fitting result of the SED is shown in Figure 4, while the marginalized posterior probability distributions of temperatures, radii, and extinction in the V band are plotted in Figure 5. When the temperatures of the primary and secondary stars converge to 7725^{+179}_{-157} K and 4404^{+189}_{-183} K, respectively, the SED model effectively describes the observed photometric data in the different bands. Additionally, the radii are $3.13^{+0.14}_{-0.15}R_\odot$ and $3.29^{+0.26}_{-0.28}R_\odot$, respectively. Therefore, in the PHOEBE fitting, we set the temperature priors of the primary and secondary stars in Gaussian distributions with expectations $\mu = 7700$ K and 4400 K and an identical standard deviation $\sigma = 200$ K, respectively.

In this work, we use subscripts 1 and 2 to describe the parameters of the primary and secondary stars, respectively. In the fitting, each component's atmosphere is modeled as a

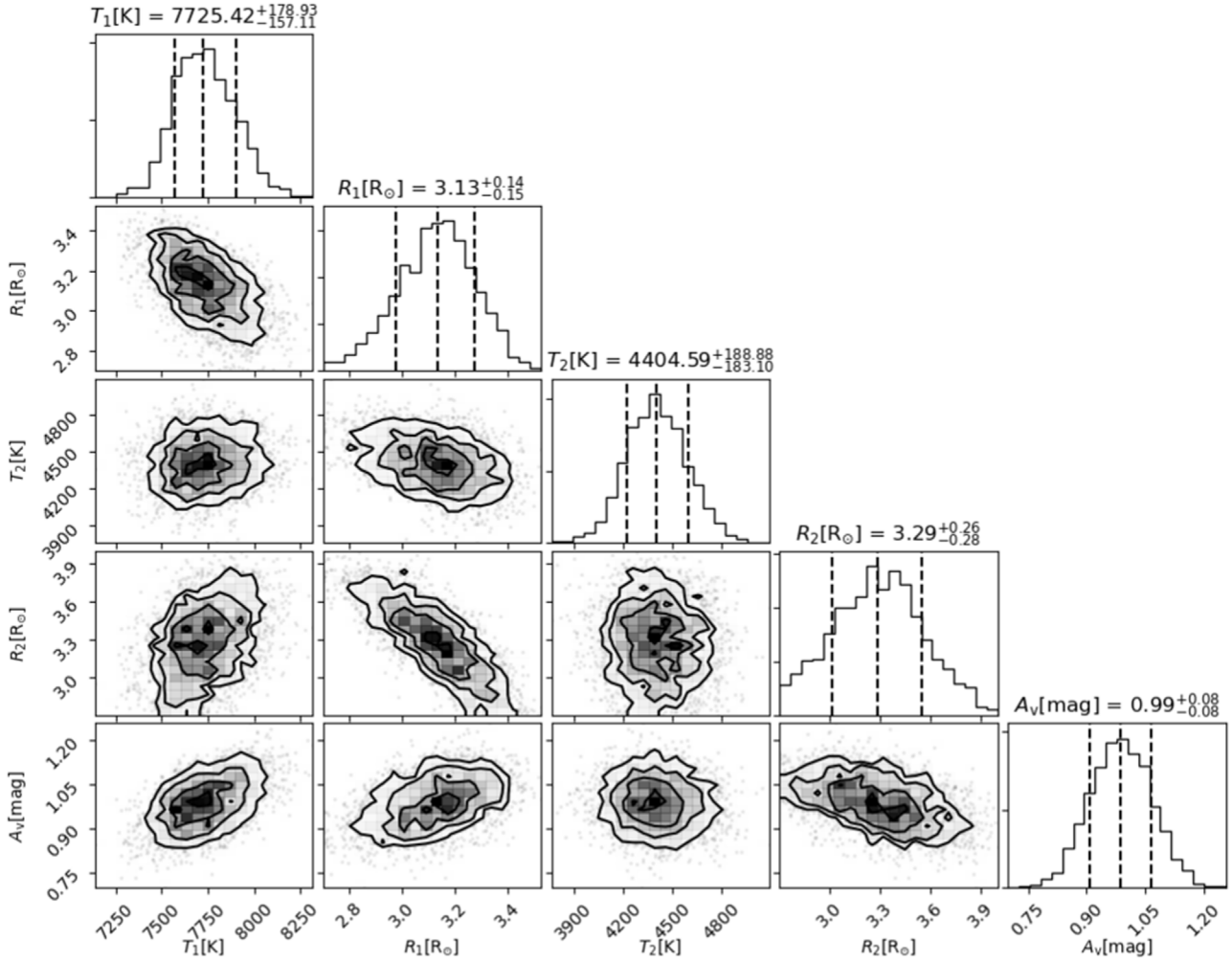

Figure 5. The marginalized posterior probability distributions of temperatures, radii, and *V*-band extinction in the SED fitting. The vertical dashed lines are located at the 16th, 50th, and 84th percentiles.

blackbody while the binary orbit is assumed as a circle with components in the tidal locking state (J. Liu et al. 2019; A. Miller et al. 2021; M. Kounkel et al. 2024), and the logarithmic limb-darkening law coefficients from A. Claret & S. Bloemen (2011) are updated automatically. The bolometric albedos are set as 1.0 and 0.5 for the primary and secondary components, respectively, while the gravity-darkening coefficients are set as fitting parameters in uniform distribution from 0.1 to 1.0. The derived orbital period $P_{\rm orb}$ remains constant with a value of $1/f_{\rm orb} = 3.12492$ days.

In Table 4, we list the prior and fitting results for the adjustable parameters, which include the orbital inclination (i), the semimajor axis (a), the mass ratio q, the mean surface temperature T_1 and T_2, the radius R_1 and R_2, and the gravity-darkening coefficients g_1 and g_2. The fitting result versus the observational light curve and the distributions of MCMC fitted parameters are shown in Figures 6 and 7, respectively. Further, based on the Kepler third law and the Stefan–Boltzmann law, we calculated the mass M_1 and M_2, surface gravity $\log g_1$ and $\log g_2$, and luminosity L_1 and L_2 and listed them in Table 4. Moreover, for a binary system with $q \leqslant 0.8$, we can determine the Roche lobe radii of the lobe-filling primary and secondary stars using Equation (4.10) in J. Frank et al. (2002). Subsequently, combining with the values of the radii of KIC 8840638, the filling factors fi_1 and fi_2 of the primary and secondary components are calculated and listed in Table 4, respectively.

For the primary component of KIC 8840638, its effective temperature $T = 7638.18^{+198.68}_{-124.68}$ K corresponds to a main-sequence star with a spectral type of about F0V $\sim$ A7V according to the relationship by P. Harmanec (1988). The filling factors fi_1 (58%) and fi_2 (89%) show that KIC 8840638 is a detached system. In addition, using the luminosities listed in Table 4, we estimate the absolute magnitude of KIC 8840638 to be 1.32 ± 0.30 mag, which is consistent with the value of 1.06 ± 0.10 mag using the distance 3174^{+137}_{-126} pc from Gaia DR3 and V magnitude.

5. Stellar Evolution Model

To investigate the formation and evolution of this binary, we employed Eggleton's stellar evolution code (Programme EV, 2012), which was originally developed by P. P. Eggleton (1971, 1972, 1973). Over the past five decades, it has undergone updates (Z. Han et al. 1994; O. R. Pols et al. 1995; C. A. Nelson & P. P. Eggleton 2001; P. P. Eggleton & L. Kiseleva-Eggleton 2002; K. Yakut & P. P. Eggleton 2005; J. J. Eldridge et al. 2008). We assumed the conservation of total mass and angular momentum for the binaries. We calculated a model grid of binary evolution with the following ranges of

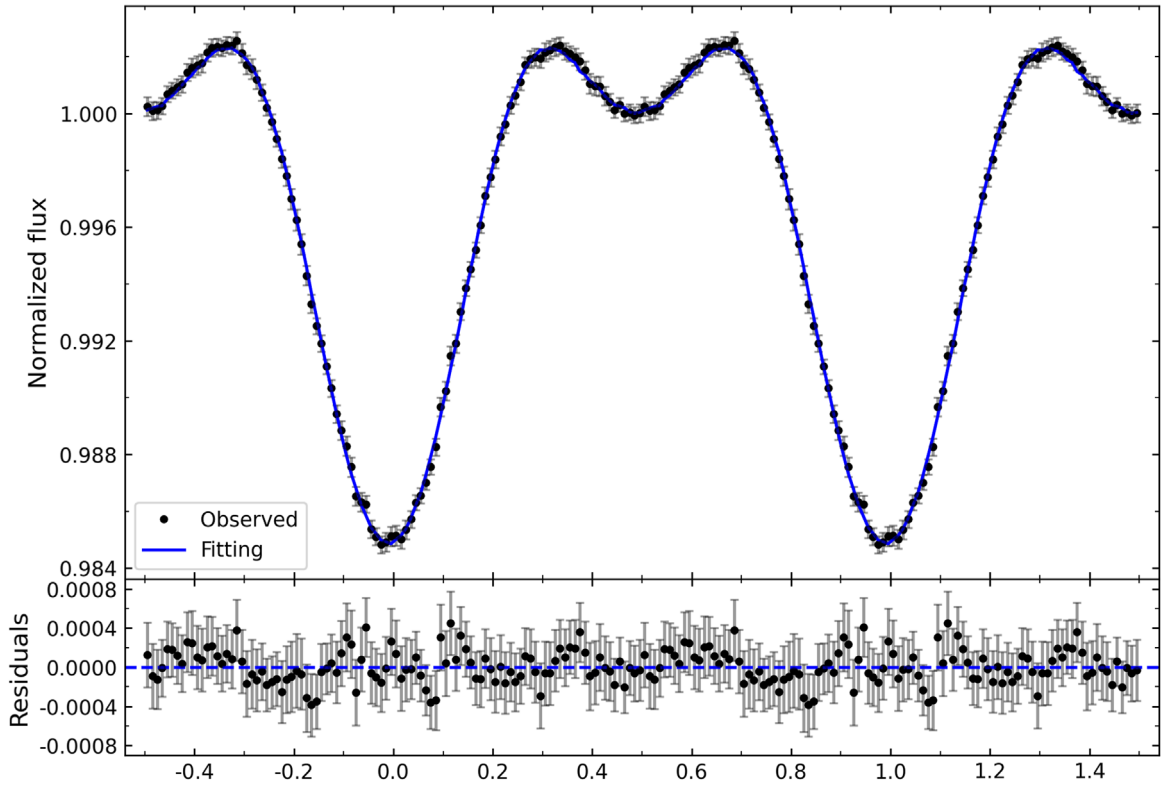

Figure 6. The normalized and phase-folded light curve of KIC 8840638 with the PHOEBE model fitting result. The corresponding residuals are plotted in the lower panel.

initial primary mass M_{10}, initial mass ratio $q_0(=M_{20}/M_{10})$, and initial orbital period P_0:

$$\log M_{10} = 0.075, 0.1, 0.125, ..., 0.2, \quad (1)$$

$$\log (1/q_0) = 0.025, 0.05, 0.075..., \ 0.15, \quad (2)$$

$$\log P_0/P_{\rm ZAMS} = 0.15, 0.175, 0.2, ..., 0.60, \quad (3)$$

where $P_{\rm ZAMS}$ is the orbital period in which the primary just fills its Roche lobe on the zero-age main sequence (C. A. Nelson & P. P. Eggleton 2001). The metallicity of these binaries was set to $Z = 0.01$, 0.02, and 0.03. These binary models evolved from the ZAMS and were terminated when both components filled their Roche lobes or the code failed to converge. By comparing the above models, we found that the evolutionary results of the model with $Z = 0.03$ are closest to the observations.

Each observed binary possesses a multitude of potential progenitors characterized by varying mass values and initial periods. In this study, the progenitor star models for the donor $S_{\rm d}$ and gainer $S_{\rm g}$ stars are identified as those that most closely match the observations on the Hertzsprung–Russell diagram (W. Van Rensbergen & J. P. De Greve 2020; W. van Rensbergen & J.-P. de Greve 2021). Comparing the results of evolutionary models with different initial values to the periods, temperatures, luminosities, and component star masses in Table 4, we suggest that the progenitor of KIC 8840638 may be a binary system with $S_{\rm d}$ and $S_{\rm g}$ having masses of 1.26 $M_\odot$ and 1.19 $M_\odot$, respectively. The metallicity and initial period are 0.03 and 0.78 day, respectively. In addition, we define the initial mass ratio of this system as $q_{\rm i} = m_{\rm d}/m_{\rm g} = 1.37$.

The evolutionary tracks of this progenitor model in $\log T_{\rm eff} - \log L$, age−mass, and age−period spaces are depicted in Figure 8 panels (1), (2) and (3), respectively. In panel (2), at around 4.712 Gyr, $S_{\rm d}$ starts transferring material to $S_{\rm g}$, accompanied by a shortening of the orbital period (as shown in panel (4)). By 4.720 Gyr, the mass of $S_{\rm d}$ becomes smaller than that of $S_{\rm g}$, indicating a reversal of the initial mass ratio, i.e., $q < 1$. As shown in panel (4), the orbital period begins to gradually lengthen from this moment. As mass transfer continues, when the progenitor star evolves to 5.593 Gyr, the orbital period of 2.952 days of the system is close to the observed one. At this point, as illustrated in panel (1), the temperature $\log T_{\rm d} = 3.66$ dex (4550 K), luminosity $\log L_{\rm d} = 0.57$ dex (3.76 $L_\odot$), and mass $M_{\rm d} = 0.49\,M_\odot$ of $S_{\rm d}$ are consistent with the PHOEBE results of the secondary star within 1σ ($T_2 = 4452.15^{+142.71}_{-138.16}$ K), 1σ ($L_2 = 3.43^{+0.57}_{-0.48}\,L_\odot$), and 1.4σ ($M_2 = 0.60^{+0.10}_{-0.08}\,M_\odot$), respectively. Similarly, for $S_{\rm g}$, the temperature $\log T_{\rm g} = 3.89$ dex (7755 K), luminosity $\log L_{\rm g} = 1.42$ dex (26.18 $L_\odot$), and mass $M_{\rm g} = 1.95\,M_\odot$ correspondingly agree with the primary star's results from PHOEBE within 1σ ($T_2 = 7638.18^{+198.68}_{-124.68}$ K), 1σ ($L_2 = 26.31^{+4.02}_{-3.12}\,L_\odot$), and 1σ ($M_2 = 1.82^{+0.12}_{-0.18}\,M_\odot$), respectively. In addition, $R_{\rm d} = 2.83\,R_\odot$ and $R_{\rm g} = 3.12\,R_\odot$ are both consistent with R_1 and R_2 within 1σ as well. From the binary evolution model, we can infer that when the progenitor star reaches an age of 5.593 Gyr, $S_{\rm d}$ and $S_{\rm g}$ might have evolved into the secondary and primary stars of the current KIC 8840638, respectively. We recall that, since there are still lots of uncertainties in binary evolution models, especially for the mass-transfer process, the evolutionary tracks may change if assumptions change. Here we only presented the best model to illustrate a typical evolution for this object. In order to further constrain the evolutionary history of KIC 8840638, direct measurements of orbital parameters (i.e., mass ratio, surface gravity, etc.) from spectra would be helpful and still needed in the future.

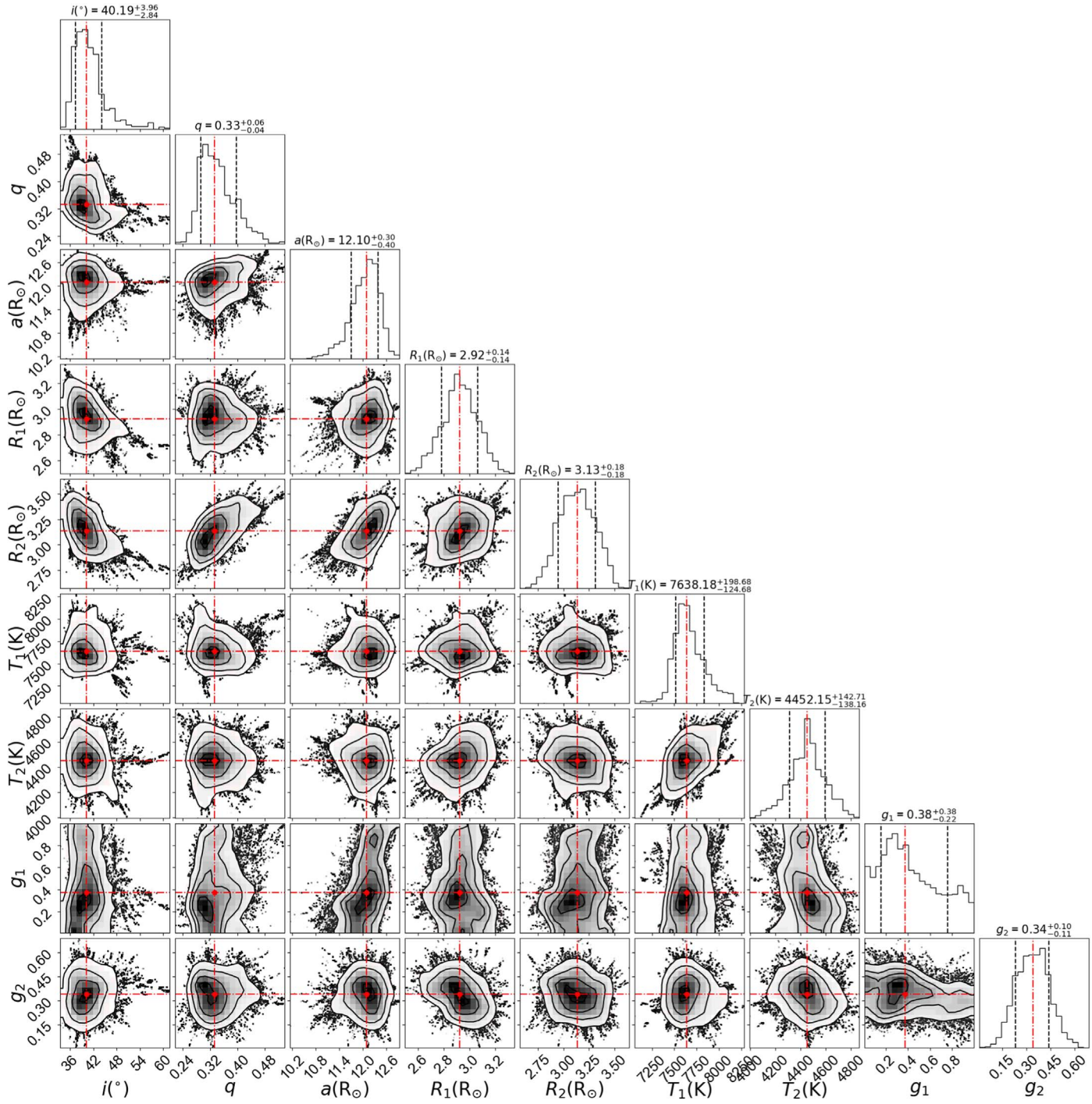

Figure 7. Model fitting parameters for the binary light curve of KIC 8840638. Corner distributions provide the posterior probabilities of the nine modifiable parameters projected in two dimensions. The vertical dashed lines in one-dimensional distributions indicate the percentiles of 16% (black dashed lines), 50% (red dashed–dotted lines), and 84% (black dashed lines), while the uncertainty displayed above corresponds to the 68th percentile. The mean value (50th percentile) of each parameter is marked with a red dot in the two-dimensional plots.

6. Discussion

To investigate the pulsating behavior of KIC 8840638, we performed a multiple-frequency analysis using the high-precision SC time-series data delivered from the Kepler mission. Among the 95 detected significant frequencies, seven stronger terms are considered as the independent modes, and they lie in the typical frequency range of δ Scuti stars. Three low frequencies ($f_1 = 0.320008\,\mathrm{day}^{-1}$, $f_3 = 0.639945\,\mathrm{day}^{-1}$, and $f_{62} = 0.959744\,\mathrm{day}^{-1}$) are also detected directly in the frequency spectrum, and the lowest frequency f_1 was identified as the orbital frequency.

Based on 69 known EBs containing δ Scuti–type components, X. B. Zhang et al. (2013) derived an upper limit of the $P_{\mathrm{pul}}/P_{\mathrm{orb}}$ ratio for δ Scuti stars in EBs with a value of 0.09, which could serve as a criterion to distinguish if a pulsating component in an EB pulsates in p-modes. For KIC 8840638, the period ratios of the above seven frequencies to the orbital

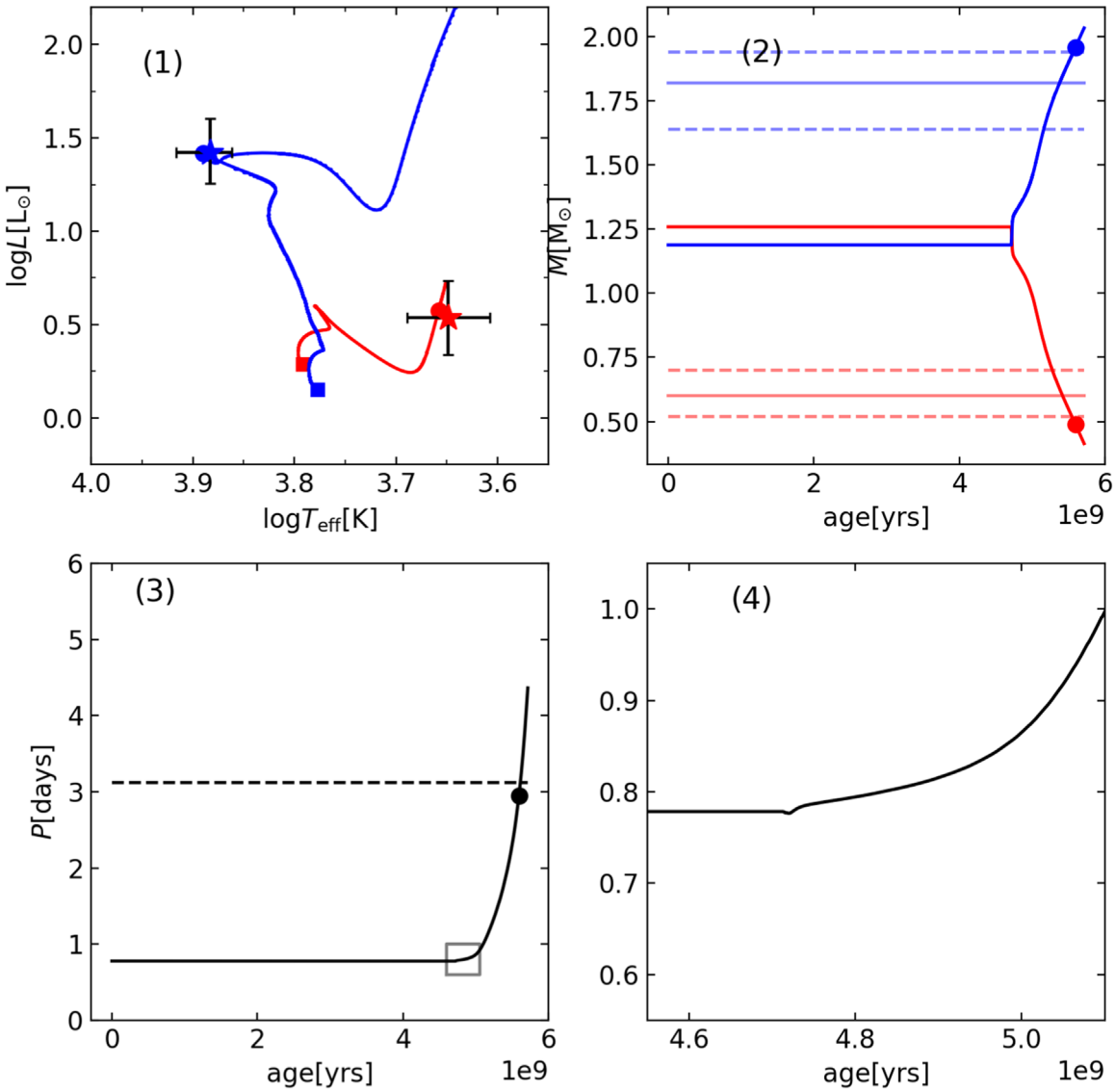

Figure 8. Evolutionary tracks of KIC 8840638. Blue lines and points represent the primary (gainer) star, while red lines and points represent the secondary (donor) star. Filled circles are located at the positions with the same age (5.59 Gyr) in the theoretical calculations. Panel (1): evolutionary tracks of the two components on the Hertzsprung–Russell diagram. Initiating from the square points, the component stars follow the theoretical evolution trajectory to the filled circles. The stars represent the PHOEBE results, and the error bars are 3 times the corresponding errors. Panel (2): theoretical mass evolution curves of the components over time. The blue straight line represents the expected value of M_1 (see Table 4), with dashed lines above and below indicating the upper and lower errors, respectively, while the red lines correspond to those parameters of M_2. Panel (3): theoretical orbital period evolution curves of the components over time. The black dashed line represents the observed period of KIC 8840638. Panel (4): a zoom-in on the initial moment (gray box in panel (3)) of the orbital period evolution caused by mass transfer.

period were calculated to be $P_{\rm pul}/P_{\rm orb} = 0.011-0.013$, which was lower than the upper limit of 0.09 for δ Scuti stars in binaries. Hence, it seems that the seven independent frequencies belong to p-modes of δ Scuti stars.

In the amplitude spectra, it can be found that most of the detected frequencies lie in a frequency region between 23.0 and 32.0 day^{-1}, which seems to show a regular frequency pattern. Hence, we tested whether the δ Sct component of the system follows the large separation ($\Delta\nu$)–mean density relation obtained by A. García Hernández et al. (2015) and improved by A. Garcia Hernandez et al. (2017). We searched for a $\Delta\nu$ pattern following the methodology described in A. García Hernández et al. (2009) and expanded in A. Ramón-Ballesta et al. (2021). It consists in calculating the FT, the histogram of frequencies (HFD), and the AC of the oscillation frequencies and makes use of an echelle diagram for the fine-tuning. A key point of the procedure is to equal the amplitudes of all the frequencies to 1 before computing any transformation. The frequencies used were listed in Table 2, but not those suspicious of being combinations. We also discarded the values above 40 day^{-1}, resulting in 61 frequencies. Their FT (in black), HFD (in gray), and AC (in blue) transformations are shown in the left panel of Figure 9. The possible value of $\Delta\nu$ is indicated by a red dotted–dashed line with a value of $\Delta\nu = 36.5 \pm 0.1$ μHz, which is the double of the higher peak in the FT and AC at around 18 μHz. The echelle diagram shown in the right panel of the figure allows us to confirm that the correct value is the double of one of the main peaks in the transformations and also to estimate the uncertainty. Using the relation $\bar{\rho}/\bar{\rho_\odot} = 1.50^{+0.09}_{-0.10}(\Delta\nu/\Delta\nu_\odot)^{2.04^{+0.04}_{-0.04}}$ by A. Garcia Hernandez et al. (2017) and this value of the large separation, we derived an expected stellar mean density of

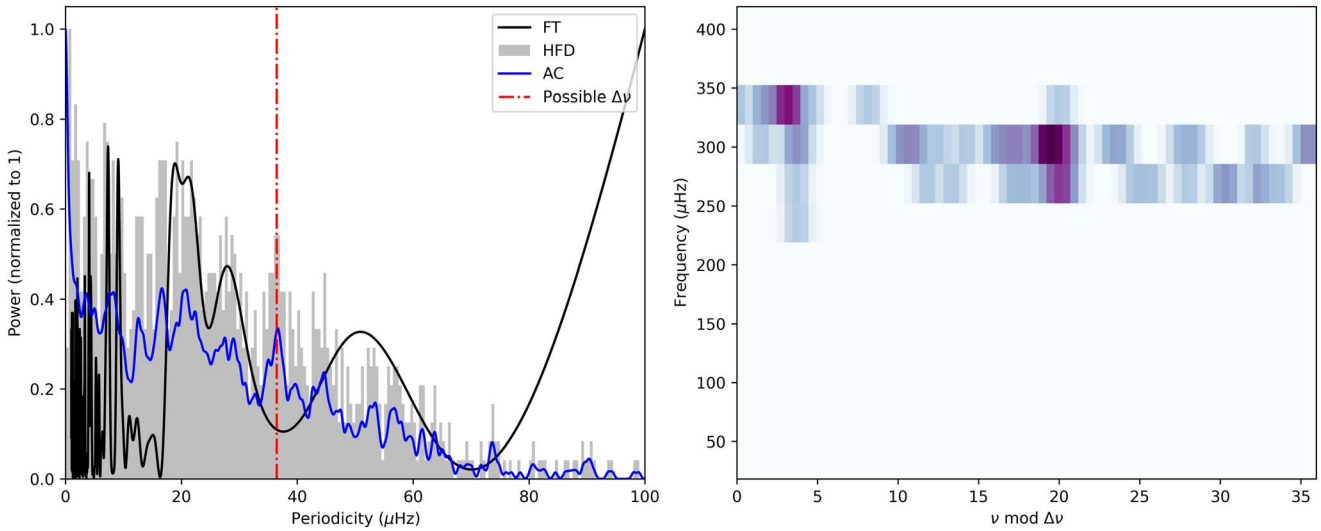

Figure 9. Left panel: FT (black), HFD (gray), and AC (blue) functions of the independent peaks lower than 40 day^{-1} found in this work. The red dotted–dashed line marks the position of $\Delta\nu = 36.5 \pm 0.1$ μHz. Right panel: echelle diagram of the frequencies showing a clear ridge around ν mod $\Delta\nu = 4\mu$Hz.

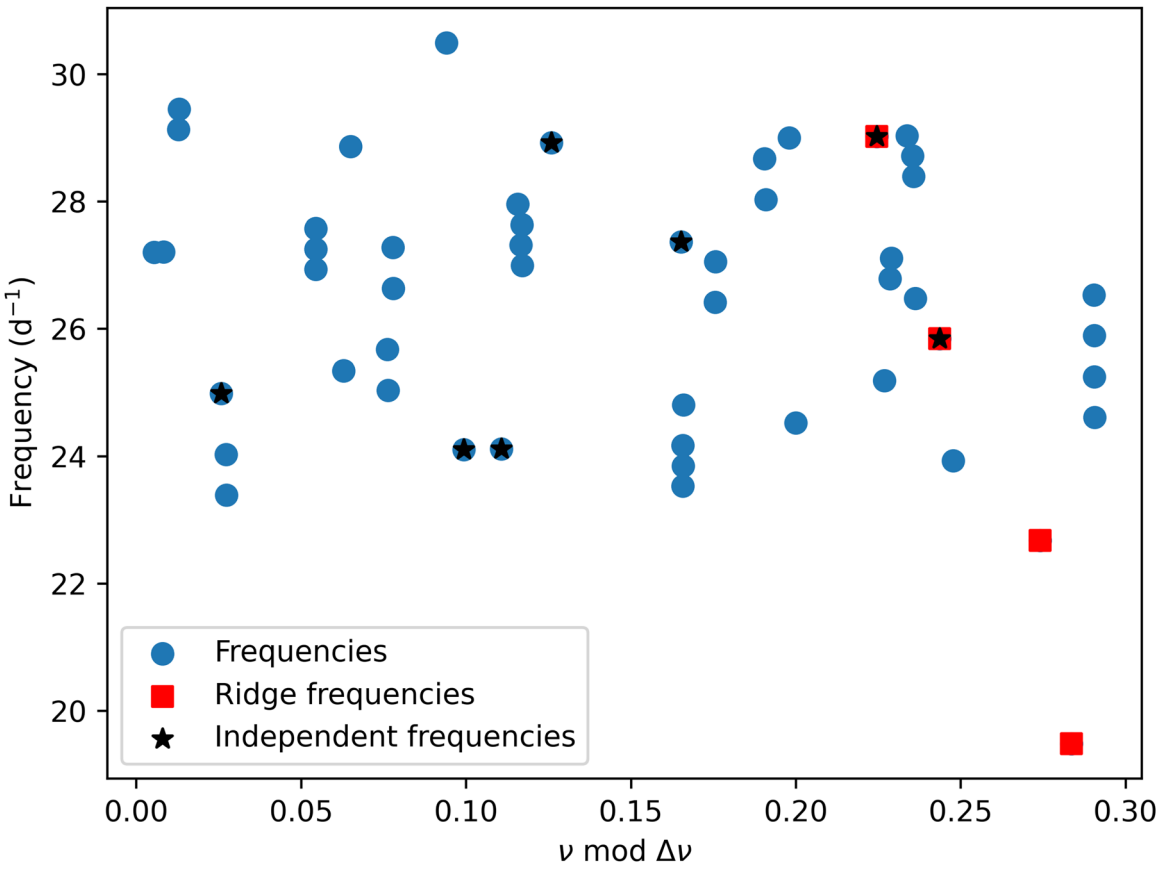

Figure 10. Echelle diagram modulo the orbital frequency.

$\rho_e = 0.148 \pm 0.012$ g cm^{-3}, which agrees within 1σ with the value $\rho = 0.136 \pm 0.019$ g cm^{-3} obtained using the mass and radius of Table 4. Despite all the evidence of a pattern corresponding to $\Delta\nu$, it has been shown that harmonics or combinations of the orbital frequencies in binary systems might hamper finding its value, as in the case of KIC 6048106 (A. Samadi Ghadim et al. 2018). To test the possibility that the pattern we found is due to tidal forces, we plotted an echelle diagram modulo the orbital frequency (see Figure 10). In this plot, the 61 frequencies used to find the large separation are depicted as blue dots, the frequencies highlighted as "independent" in Table 2 are represented as black stars, and those forming the main ridge of the large separation are represented as red squares. As can be noticed, we have still missed some frequencies that can be a harmonic of the orbital frequency. However, these are not the frequencies in the $\Delta\nu$ ridge. Moreover, the seven independent frequencies are neither harmonic nor combinations of the value of $\Delta\nu$ between F2

and F4, for example, the highest amplitude peaks after $f_{\rm orb}$. Thus, we discard that $\Delta\nu = 36.5\ \mu{\rm Hz} = 3.15\ {\rm day}^{-1}$ is due to tidal forces.

To obtain the parameters of the binary system, we modeled the smoothed light curve of KIC 8840638 using the PHOEBE package. From light-curve synthesis, this target is a detached EB system with configurations of $q = 0.33^{+0.06}_{-0.04}$, an inclination angle of $40.19^{+3.96}_{-2.84}{}^{\circ}$, and a temperature difference of ∼3100 K between the two components. The primary component fills $fi_1 = 58^{+3}_{-3}\%$ of its inner critical lobe, while the secondary fills $fi_2 = 89^{+3}_{-4}\%$ of its inner critical lobe, also implying that KIC 8840638 would be a detached system.

By utilizing the stellar evolution model (Section 5), we obtained theoretical parameters that are self-consistent with the results of PHOEBE's light-curve fitting solution, i.e., temperatures, masses, and luminosities of the components. We infer that the progenitor star of KIC 8840638 may be a binary system with initial masses of $M_{\rm d} = 1.26\,M_{\odot}$ and $M_{\rm g} = 1.19\,M_{\odot}$ and an initial period of 0.78 day. The donor star filled its Roche lobe around 4.712 Gyr, initiating mass transfer to the gainer star. After about 0.008 Gyr, the mass ratio between the two stars became 1, marking the beginning of the mass ratio reversal phase (i.e., the mass ratio started to be less than 1). Finally, at 5.593 Gyr, the progenitor system likely evolved into KIC 8840638, as observed today.

7. Conclusions

In this paper, we investigated the light variation of KIC 8840638 using the Kepler SC time-series data obtained from quarters 14–17. The analysis of light curves suggests that this target is a new pulsating EB system, rather than a single pulsating star as previously known. With Fourier transformation of light curves, we detected 95 significant frequencies, seven of which are identified as independent p-modes in the frequency range of $23.0-32.0\ {\rm day}^{-1}$. In addition, a possible large separation value of $\Delta\nu = 36.5 \pm 0.1\ \mu$Hz is also detected using the FT and AC analysis.

To investigate the binary parameters of this target, we constructed binary modelings using the Kepler light curve. The synthetic light curves suggest that this binary is a detached EB system with $q = 0.33^{+0.06}_{-0.04}$, an inclination angle of $40.19^{+3.96}_{-2.84}{}^{\circ}$, and a temperature difference of nearly 3100 K between the two components. According to the stellar evolution model, it is evident that this system may have undergone a mass ratio reversal. Currently, in KIC 8840638, the larger-mass star is the gainer star, while the smaller-mass star is the donor star. Moreover, the primary star of the system may be located at the edge of leaving the main sequence, while the secondary star is likely situated on the giant branch.

Regarding any future studies of KIC 8840638, it could be mentioned that radial velocity measurements will certify or modify the values of the absolute parameters, such as mass and surface gravity. Considering it is faint ($K_P = 14.262$ mag), high-resolution spectrographs in telescopes with diameters of 8–10 m are needed to detect signals of both components.

Acknowledgments

We are grateful to the anonymous referee for providing thoughtful and helpful comments that improved the manuscript. This research is supported by the program of the National Natural Science Foundation of China (grant Nos. 12003020, 12473043) and Shaanxi Fundamental Science Research Project for Mathematics and Physics (grant No. 23JSY015). A.G.H. acknowledges funding support from the Spanish State Research Agency (AEI) project PID2019-107061GB-064. We would like to thank the Kepler science team for providing such excellent data. D.J. acknowledges support from the National Key R&D Program of China No. 2021YFA1600403, the National Natural Science Foundation of China (Nos. 12473033,12073070, 12333008, 12288102, 12090040/3), the Western Light Project of CAS (No. XBZG-ZDSYS-202117), International Centre of Supernovae, Yunnan Key Laboratory (No. 202302AN360001), Yunnan Fundamental Research Project (No. 202201BC070003, 202401BC070007), Yunnan Revitalization Talent Support Program—Science & Technology Champion Project (No. 202305AB350003), Yunnan Ten Thousand Talents Plan Young & Elite Talents Project, and the China Manned Space Project with No. CMS-CSST-2021-A08.

ORCID iDs

Tao-Zhi Yang https://orcid.org/0000-0002-1859-4949
Zhao-Yu Zuo https://orcid.org/0000-0001-6693-586X
Jun-Hui Liu https://orcid.org/0000-0002-7600-1670
Deng-Kai Jiang https://orcid.org/0000-0003-4265-7783
Zhi-Xiang Zhang https://orcid.org/0000-0002-2419-6875
Antonio García Hernández https://orcid.org/0000-0002-6906-4526

References

Abazajian, K. N., Adelman-McCarthy, J. K., Agüeros, M. A., et al. 2009, ApJS, 182, 543
Allard, F., Homeier, D., & Freytag, B. 2012, RSPTA, 370, 2765
Balona, L. A. 2014, MNRAS, 437, 1476
Balona, L. A., & Dziembowski, W. A. 2011, MNRAS, 417, 591
Borucki, W. J., Koch, D., Basri, G., et al. 2010, Sci, 327, 977
Bowman, D. M., Kurtz, D. W., Breger, M., Murphy, S. J., & Holdsworth, D. L. 2016, MNRAS, 460, 1970
Breger, M. 2000, in ASP Conf. Ser. 210, Delta Scuti and Related Stars, ed. M. Breger & M. Montgomery (San Francisco, CA: ASP), 3
Breger, M., Stich, J., Garrido, R., et al. 1993, A&A, 271, 482
Brown, T. M., Latham, D. W., Everett, M. E., & Esquerdo, G. A. 2011, AJ, 142, 112
Cardelli, J. A., Clayton, G. C., & Mathis, J. S. 1989, ApJ, 345, 245
Chambers, K. C., Magnier, E. A., Metcalfe, N., et al. 2016, arXiv:1612.05560
Chen, X., Ding, X., Cheng, L., et al. 2022, ApJS, 263, 34
Chen, X., Zhang, X., Li, Y., et al. 2020, ApJ, 895, 136
Chen, X., Zhang, X., Li, Y., et al. 2021, ApJ, 920, 76
Claret, A., & Bloemen, S. 2011, A&A, 529, A75
Clausen, J. V., Torres, G., Bruntt, H., et al. 2008, A&A, 487, 1095
Cutri, R. M., Wright, E. L., Conrow, T., et al. 2021, yCat, 2328, 0
Eggleton, P. P. 1971, MNRAS, 151, 351
Eggleton, P. P. 1972, MNRAS, 156, 361
Eggleton, P. P. 1973, MNRAS, 163, 279
Eggleton, P. P., & Kiseleva-Eggleton, L. 2002, ApJ, 575, 461
El-Badry, K., & Rix, H.-W. 2022, MNRAS, 515, 1266
Eldridge, J. J., Izzard, R. G., & Tout, C. A. 2008, MNRAS, 384, 1109
Fitzpatrick, E. L. 1999, PASP, 111, 63
Foreman-Mackey, D., Hogg, D. W., Lang, D., & Goodman, J. 2013, PASP, 125, 306
Frank, J., King, A., & Raine, D. J. 2002, Accretion Power in Astrophysics (3rd ed.; Cambridge: Cambridge Univ. Press), 398
Gaia Collaboration, Vallenari, A., Brown, A. G. A., et al. 2023, A&A, 674, A1
García Hernández, A., Martín-Ruiz, S., Monteiro, M. J. P. F. G., et al. 2015, ApJL, 811, L29
García Hernández, A., Moya, A., Michel, E., et al. 2009, A&A, 506, 79
Garcia Hernandez, A., Suarez, J. C., Moya, A., et al. 2017, MNRAS, 471, L140

Green, G. M., Schlafly, E., Zucker, C., Speagle, J. S., & Finkbeiner, D. 2019, ApJ, 887, 93
Guo, Z., Gies, D. R., Matson, R. A., et al. 2017, ApJ, 837, 114
Hambleton, K. M., Kurtz, D. W., Prsa, A., et al. 2013, MNRAS, 434, 925
Han, Z., Podsiadlowski, P., & Eggleton, P. P. 1994, MNRAS, 270, 121
Harmanec, P. 1988, BAICz, 39, 329
Henden, A. A., Levine, S., Terrell, D., & Welch, D. L. 2015, AAS Meeting, 225, 336.16
Hilditch, R. W. 2001, An Introduction to Close Binary Stars (Cambridge: Cambridge Univ. Press), 392
Houdek, G., Balmforth, N. J., Christensen-Dalsgaard, J., & Gough, D. O. 1999, A&A, 351, 582
Huber, D., Silva Aguirre, V., Matthews, J. M., et al. 2014, ApJS, 211, 2
Kahraman Alicavus, F., Soydugan, E., Smalley, B., & Kubat, J. 2017, MNRAS, 470, 915
Kallinger, T., Reegen, P., & Weiss, W. W. 2008, A&A, 481, 571
Kirk, B., Conroy, K., Prša, A., et al. 2016, AJ, 151, 68
Kjeldsen, H., Christensen-Dalsgaard, J., Handberg, R., et al. 2010, AN, 331, 966
Koch, D. G., Borucki, W. J., Basri, G., et al. 2010, ApJL, 713, L79
Kounkel, M., Statti, M., Kulkarni, A., Stassun, K. G., & Sun, M. 2024, MNRAS, 527, 3806
Kreiner, J. M., Kim, C.-H., & Nha, I.-S. 2001, An Atlas of O-C Diagrams of Eclipsing Binary Stars (Cracow: Wydawnictwo Naukowe Akademii Pedagogicznej)
Lee, J. W., Hong, K., Kim, S.-L., & Koo, J.-R. 2016, MNRAS, 460, 4220
Lee, J. W., Hong, K., Kim, S.-L., & Koo, J.-R. 2017, ApJ, 835, 189
Lee, J. W., Hong, K., & Kristiansen, M. H. 2019, AJ, 157, 17
Lenz, P., & Breger, M. 2005, CoAst, 146, 53
Liakos, A. 2018, A&A, 616, A130
Liakos, A., & Niarchos, P. 2015, in ASP Conf. Ser. 496, Living Together: Planets, Host Stars and Binaries, ed. S. M. Rucinski, G. Torres, & M. Zejda (San Francisco, CA: ASP), 195
Liakos, A., & Niarchos, P. 2016, arXiv:1606.08638
Liakos, A., & Niarchos, P. 2017, MNRAS, 465, 1181
Liu, J., Esamdin, A., Zhang, Y., et al. 2019, PASP, 131, 084202
Miller, A., Kounkel, M., Sun, M., et al. 2021, AJ, 162, 131
Mkrtichian, D. E., Kusakin, A. V., Rodriguez, E., et al. 2004, A&A, 419, 1015
Nelson, C. A., & Eggleton, P. P. 2001, ApJ, 552, 664
Pols, O. R., Tout, C. A., Eggleton, P. P., & Han, Z. 1995, MNRAS, 274, 964
Popper, D. M. 1980, ARA&A, 18, 115
Prša, A., Conroy, K. E., Horvat, M., et al. 2016, ApJS, 227, 29
Prša, A., & Zwitter, T. 2005, ApJ, 628, 426
Ramón-Ballesta, A., García Hernández, A., Suárez, J. C., et al. 2021, MNRAS, 505, 6217
Ramsay, G., Brooks, A., Hakala, P., et al. 2014, MNRAS, 437, 132
Rodríguez, E., & Breger, M. 2001, A&A, 366, 178
Samadi Ghadim, A., Lampens, P., & Jassur, M. 2017, MNRAS, 474, 5549
Skrutskie, M. F., Cutri, R. M., Stiening, R., et al. 2006, AJ, 131, 1163
Southworth, J., Smalley, B., Maxted, P. F. L., Claret, A., & Etzel, P. B. 2005, MNRAS, 363, 529
Soydugan, E., Ibanoglu, C., Soydugan, F., Akan, M. C., & Demircan, O. 2006, MNRAS, 366, 1289
Stassun, K. G., Oelkers, R. J., Paegert, M., et al. 2019, AJ, 158, 138
Sun, X.-Y., Zuo, Z.-Y., Yang, T.-Z., & García Hernández, A. 2023, ApJ, 955, 80
Torres, G., Andersen, J., & Giménez, A. 2010, A&ARv, 18, 67
Van Rensbergen, W., & De Greve, J. P. 2020, A&A, 642, A183
van Rensbergen, W., & de Greve, J.-P. 2021, Galax, 9, 19
Welsh, W. F., Orosz, J. A., Aerts, C., et al. 2011, ApJS, 197, 4
Yakut, K., & Eggleton, P. P. 2005, ApJ, 629, 1055
Yang, T., Esamdin, A., Song, F., et al. 2018, ApJ, 863, 195
Yang, T.-Z., & Esamdin, A. 2019, ApJ, 879, 59
Yang, T.-Z., Sun, X.-Y., Zuo, Z.-Y., & Liu, H.-W. 2021, AJ, 161, 27
Yang, T.-Z., Zuo, Z.-Y., Sun, X.-Y., Tang, R.-X., & Esamdin, A. 2022, ApJ, 936, 48
Zacharias, N., Finch, C. T., Girard, T. M., et al. 2012, yCat, 1322, 0
Zacharias, N., Finch, C. T., Girard, T. M., et al. 2013, AJ, 145, 44
Zhang, X. B., Luo, C. Q., & Fu, J. N. 2013, ApJ, 777, 77